PE/OMMT Nanocomposites Prepared by *In Situ* Polymerization Approach: Effects of OMMT-Intercalated Catalysts and Silicate Modifications

Ying-Juan Huang,[1,2] Ya-Wei Qin,[1] Jin-Yong Dong,[1] Xutao Zhao,[3] Xuteng Hu[3]

[1]*CAS Key Laboratory of Engineering Plastics, Institute of Chemistry, Chinese Academy of Sciences, Beijing, People's Republic of China*
[2]*Graduate School of Chinese Academy of Sciences, Beijing, People's Republic of China*
[3]*Petrochemical Research Institute, PetroChina Company Ltd, Beijing 100190, China*

Received 13 December 2009; accepted 18 May 2011
DOI 10.1002/app.34939
Published online 2 September 2011 in Wiley Online Library (wileyonlinelibrary.com).

ABSTRACT: In this article, the surfactants, (2-hydroxylethyl) octadecyl dimethylammonium nitrate (OH-C18), hexadecyltrimethylammonium bromide(C16), and mixture of trimethylchlorosilane (TM) and OH-C18 were ion-exchanged with cations in the montmorillonite (MMT) to generate three organic MMTs (named as OH-C18-MMT, C16-MMT, and MMMT), leading to different environments of catalyst species in MMT interlayer gallery. Et[Ind]$_2$ZrCl$_2$ (abbreviated as EI) was supported on the above three types of OMMTs to prepare the PE/OMMT nanocomposites via *in situ* polymerization. By contrast, EI/MMMT showed higher activity than EI/OH-C18-MMT and EI/C16-MMT under the same polymerization conditions. The other two types of catalysts, such as [(*tert*-Bu)NSi(Me$_2$)C$_5$Me$_4$]TiCl$_2$ (CGCT) and Bis[N-(3-*tert*-butylsalicylidene)anilinato] titanium (IV) dichloride (FI) were also supported on the OH-C18-MMT for *in situ* ethylene polymerization. It was found that the activity of FI/OH-C18-MMT for ethylene polymerization was much lower than the other two corresponding catalysts under the similar reaction conditions. © 2011 Wiley Periodicals, Inc. J Appl Polym Sci 123: 3106–3116, 2012

Key words: PE/OMMT nanocomposites; FI; EI; CGCT; trimethylchlorosilane

INTRODUCTION

Since the invention of nylon-6/montmorillonite (MMT) nanocomposites with impressive material properties by Toyota researchers in the early 1990s,[1] the research on these polymer/inorganic nano-phase composites was revived and attracted a considerable interest. This is because the introduction of a few weight percent of nanometer-scale laminated silicate layers into a polymer matrix can drastically improve many polymer properties, such as modulus, strength, heat resistance, antiflammability, and anti-gas permeability, which are usually very difficult to access by traditional micrometer-scale inorganic fillers.[2]

Polyolefins (PE, PP, etc.) are among the most interesting polymers, which are deemed to benefit the most from the information of nanocomposites with MMT due to their wide range of applications.[3] However, polyolefins are of chemically nonpolar character, which dictates its nearly complete immiscibility with inorganic MMT and poses great challenges for the preparation of polyolefin/MMT nanocomposites by direct polymer intercalation method (including melt and solution intercalations). The *in situ* intercalative polymerization has been one effective approach, which is conducted by the intercalation of transition metal olefin polymerization catalysts (including Ziegler-Natta, metallocene, and postmetallocene) in the interlayer of an organically modified MMT (OMMT) followed by an *in situ* olefin polymerization. There is abundant evidence available to show it is more desirable in terms of effectiveness to form nanocomposite structures than a melt or solution polymer intercalation assisted by a functional polyolefin compatibilizer.[4–7]

For *in situ* polymerization technique, the most important step is the fixation of the catalyst in between the silicate layers of MMT,[8,9] because the interlayer distance of the silicate layers determines the ease of

Correspondence to: J.-Y. Dong (jydong@iccas.ac.cn).
Contract grant sponsor: National Science Foundation of China; contract grant numbers: 20734002, 20874104, and 51003106.
Contract grant sponsor: Ministry of Science and Technology of China (863 project); contract grant numbers: 2008AA030901, 2009AA033601.
Contract grant sponsor: Chinese Academy of Sciences (Directional key project on high performance polypropylene alloy resin development).

catalyst approaching to active sites. Olefin polymerization catalysts supported on the inorganic support usually exhibit lower activities compared to nonsupported catalysts.[10,11] Some researchers[12–20] reported that the nanoscale silicate layers of OMMT were dispersed into the final polyolefin/OMMT nanocomposites catalyzed by those catalysts supported on the OMMT. Notable examples are Ziegler-Natta catalysts,[9] metallocene catalysts,[12–14] and late transition metal-based catalysts.[15–17] Kwak and coworkers reported $TiCl_4$ into galleries of montmorillonite modified with methyl tallow bis(2-hydroxyethyl) quaternary ammonium moiety to prepare PE/OMMT nanocomposites with a complete exfoliation of the layered silicates.[9] Wang et al. prepared PE/OMMT nanocomposites catalyzed by the $(n\text{-BuCp})_2ZrCl_2$/MMT catalyst, and it was concluded that the silicate layers became gradually exfoliated as the polymerization time increased.[12] Tang and coworkers used the single-component Cp_2ZrCl_2 catalyst supported on the MMT modified by (3-aminopropyl)triethoxysilane for ethylene polymerization and found a surprising result that the (co)polymers from the Cp_2ZrCl_2 / OMMT catalysts are bimodal in MWD.[13] Alexander et al. synthesized PE-silicate nanocomposites with good exfoliation by the *in situ* polymerization of ethylene with a constrained geometry catalyst (CGC) [(*tert*-butylamido)dimethyl(tetramethyl-5-cyclopentadienyl) silane titanium(IV) dimethyl] supported on montmorillonite, hectorite, and kaolin for comparative studies.[14] Heinemann et al. reported to produce PE/silicate nanocomposites catalyzed by metallocene Me_2Si(2-methylbenz[*e*]indenyl)$_2ZrCl_2$, nickel catalysts *N,N*-bis(2, 6-diisopropylphenyl)-1,4-diaza-2,3-dimethyl-1,3- butadienenickel, and palladium catalyst $\{[ArNAC(Me)OC(Me)ANAr]\ Pd(CH_3)(NCOCH_3)\}^+BAr_4^-$ intercalated in Na-bentonites modified with dimethyldistearylammonium or dimethylbenzylstearylammonium cations, respectively.[15] Sivaram and coworkers chose 2,6-bis[1-(2,6-diisopropylphenylimino)ethyl] pyridine iron(II) dichloride supported on a modified montmorillonite clay to prepare the PE/OMMT nanocomposites. They obtained the exfoliating PE/OMMT nanocomposites and concluded that at least some of the active centers reside within the galleries of the clay.[16] Coates and coworkers reported that Brookhart's single component palladium-based complex $\{[\{2,6\text{-}Pri_2C_6H_3NNC(Me)C\text{-}(Me)NNC_6H_3Pri_2\text{-}2.6\}Pd(CH_2)_3CO_2Me]\ [B(C_6H_3(CF_3)_2\text{-}3,5)_4]\}$ was intercalated into the synthetic silicate fluorohectorite as the ethylene polymerization catalyst to prepare PE/OMMT nanocomposites with good exfoliation of OMMT.[17] Recently, Tritto and coworkers prepared highly filled PE-based hybrids with a homogeneous distribution of the clay by *in situ* polymerization technique,[18] and further produced low-filled and well-dispersed PE/clay nanocomposites.[19] They concluded that the property of PE as well as the morphology of the nanocomposites could be tuned by varying the nature of the inorganic support, 2,6-bis(imnio)pyridyl iron(II) catalytic systems, the clay pretreatment, and experimental polymerization conditions.

In our previous research, Ziegler-Natta catalysts[20,21] or metallocene catalysts[22–24] were supported on OMMT to prepare the polyolefin/OMMT nanocomposites with well-exfoliated and homogenously dispersed OMMT. As a part of our follow-up research, three different surfactants, trimethylchlorosilane, (2-hydroxylethyl) octadecyl dimethylammonium nitrate, and hexadecyl trimethylammonium bromide were used to modify Na-MMT. The organic MMTs with a single functional group (-OH) surfactant of (2-hydroxylethyl) octadecyl dimethylammonium nitrate and a nonfunctional group surfactant of hexadecyl trimethylammonium bromide were remarked as OH-C18-MMT and C16-MMT, respectively. The organic MMT modified by a mix of trimethylchlorosilane and (2-hydroxylethyl) octadecyl dimethylammonium nitrate was named as MMMT. $Et[Ind]_2ZrCl_2$ (abbreviated as EI) was supported on the above three types of OMMTs to prepare the PE/OMMT nanocomposites via *in situ* polymerization technique. EI and $[(tert\text{-Bu})NSi(Me_2)C_5Me_4]TiCl_2$ (abbreviated as CGCT) catalysts, as two of highly active group 4 metallocene catalysts, have been commercially successful for preparing polyethylene, isotactic, and syndiotactic polypropylene (*i*-PP, *s*-PP). And Bis[N-(3-*tert*-butylsalicylidene)anilinato] titanium(IV) dichloride (abbreviated as FI), as one type of postmetallocene catalyst based on transition metal complexes, displays the excellent catalytic performance and so has very high potential as a new generation of olefin polymerization catalysts.[25] Both CGCT and FI catalysts supported on OH-C18-MMT were also investigated for ethylene polymerization to obtain PE-based hybrids in this article.

EXPERIMENTAL

Materials and instruments

All O_2- and moisture-sensitive manipulations were carried out inside an argon-filled Vacuum Atmosphere dry-box equipped with a dry train. Chemically pure-grade toluene was deoxygenated by argon purge prior to be refluxed for 48 h and distilled over sodium. Trimethylchlorosilane (C_3H_9ClSi), (2-hydroxylethyl) octadecyl dimethylammonium nitrate ($C_{22}H_{48}N_2O_4$) and hexadecyl trimethylammonium bromide surfactant ($C_{19}H_{42}Br$) surfactant were purchased from Beijng Jingxi Chemical Factory. Methylaluminoxane (MAO) (1.4*M* in toluene) was

purchased from Albermarle and used as received. Et[Ind]$_2$ZrCl$_2$ (EI) and [(*tert*-Bu)NSi(Me$_2$)C$_5$Me$_4$]TiCl$_2$ (CGCT) were purchased from Aldrich. Bis[N-(3-*tert*-butylsalicylidene)anilinato]titanium(IV) dichloride (FI) was synthesized according to the literature.[25]

Polymerization-grade ethylene was supplied by Yanshan Petrochemical Co. of China. The original Na-MMT was produced by Qinghe Chemical Plant (China) with a cation exchange capacity (CEC) of 100 mequiv (100 g)$^{-1}$.

Organic modification of Na-MMT

MMT (10 g) and trimethylchlorosilane (12 g) were mixed in acetone (100 mL) and refluxed for 36 h under stirring conditions. The product was filtered and washed with acetone twice and then washed with 95% ethanol for several times to make sure that the product contained no Cl^- (no white precipitate was detected by 0.1*M* aqueous $AgNO_3$ solution in the filtrate). The product was dried for 8 h at 100°C in vacuum and then ground to get 8.5 g chlorosilane-modified clay (remarked as TMA).

Clay (Na-MMT or TMA, 10 g) was ion-exchanged with (2-hydroxylethyl) octadecyl dimethylammonium nitrate ($C_{22}H_{48}N_2O_4$) (5.0 g) in 500 mL of the mixed solvent (ethanol : H_2O = 1 : 1 weight) at 60°C for 24 h under agitation. The precipitate was collected by filtration and washed with hot water and ethanol several times until no NO_3^- could be detected after stirring was stopped. The precipitate was dried in vacuum at 60°C for 24 h and 9.7g product was grounded to powder (sample of Na-MMT and TMA ion-exchanged with the surfactant was remarked as OH-C18-MMT and MMMT, respectively). The yield of OH-C18-MMT was 9.8 g. The preparation of C16-MMT followed the same procedure as that of OH-C18-MMT, only the surfactant was replaced by hexadecyl trimethylammonium bromide surfactant alone (remarked as C16-MMT). 8.9 g of C16-MMT was obtained.

Synthesis of the OMMT-intercalated catalyst

In a typical reaction (EI/OH-C18-MMT), to a 250-mL three-necked flask containing 5.3 g of OH-C18-MMT was added 100 mL of toluene at 60°C. The mixture was stirred for 2 h before 20 mL of MAO was introduced into the flask. After stirring for 12 h, 0.6 mmol of *rac*-Et[Ind]$_2$ZrCl$_2$ in 40 mL MAO solution was added by syringe into the flask. The reaction was allowed to proceed for 10 h. After the reaction was complete, the reactants were subjected to filtration, repeated washing with toluene (5 × 50 mL), and drying under vacuum at 60°C to give the OH-C18-MMT-intercalated Et[Ind]$_2$ZrCl$_2$ catalyst (abbreviated as EI/OH-C18-MMT) as a gray powder. Likewise, the OH-C18-MMT-intercalated [(*tert*-Bu)NSi(Me$_2$)C$_5$Me$_4$]TiCl$_2$ (CGCT) and Bis[N-(3-*tert*-butylsalicylidene)anilinato] titanium(IV) dichloride catalysts were prepared following the same procedure, respectively.

Preparation of PE/OMMT nanocomposites

The polymerization reactions were carried out with a Parr stainless steel autoclave reactor equipped with a mechanical stirrer. In a typical reaction (entry S2 in Table I), 50 mL hexane was introduced into the reactor. The reactor was then filled with ethylene under a constant pressure of 0.5 MPa. After the reactor had been heated to 50°C, the powdery EI/OH-C18-MMT catalyst (0.116 g) was added into the vigorously stirred liquid mixture saturated with ethylene. The polymerization reaction was initiated by charging 2.9 mL of MAO (4.03 mmol) into the reactor using a syringe. After 30 min, the polymerization was quenched by 20 mL of acidified ethanol (containing 10% of HCl). The polymer product was collected by filtration and repeatedly washed with ethanol. After drying under vacuum at 60°C for 24 h, 6.73 g of polymer product was obtained in white powder (PE/OMMT).

Characterization

The melting temperatures of the polymers were measured by differential scanning calorimetry (DSC) using a Perkin–Elmer Pyris 1 instrument. All specimens were heated from 50 to 180°C at heating rate of 10°C/min and kept for 5min to eliminate the thermal history. The melt and crystallization behavior was then recorded at heating or cooling rate of 10°C/min. And the melting temperature (T_m) was determined at the second heating scan.

Thermogravimetric analysis (TGA) was performed on a Perkin–Elmer TGA instrument in nitrogen atmosphere under a flow rate of 50 mL/min with a heating range of 50–700°C and a heating rate of 20°C/min. The inorganic content in the hybrid composites was determined by the residue observed at 600°C.

Wide-angle X-ray diffraction (WAXD) was performed on a D8 advance X-ray powder diffractometer (Bruker Co.) with Cu Ka radiation (λ = 0.15406 nm) at a generator voltage of 40 kV and generator current of 40 mA. The scanned 2θ range was from1.5° to 40° with a scanning rate of 4°/min. The interlayer spacing (d001) of MMT was calculated in accordance with the Bragg equation: $2d\sin\theta = \lambda$. The powder-polymerized samples were compressed at room temperature before being evaluated by WAXD.

TABLE I
A Summary of Conditons[a] and Results of Ethylene Polymerization Using EI/OH-C18-MMT, EI/MMMT, and EI/C16-MMT

Entry.	[MAO]/[Zr] (mol/mol)	T (°C)	t (min)	Yield (g)	A[b]	MMT[c] (wt %)	T_m (°C)
Homogeneous EI							
PE1[d]	1000	50	30	12.9	25.8	–	131.4
EI/OH-C18-MMT							
S1	500	50	30	3.11	1.51	3.8	132.5
S2	1000	50	30	6.73	3.34	2.8	133.3
S3	1700	50	30	7.17	3.66	1.5	133.0
S4	3400	50	30	12.82	6.33	0.9	134.8
S5	1000	30	30	1.33	0.64	9.8	133.2
S6	1000	50	60	5.05	1.29	2.2	132.9
EI/MMMT							
T1	500	50	30	7.13	3.66	3.2	131.6
T2	1000	50	30	8.19	4.14	2.8	134.0
T3	1700	50	30	8.68	4.29	2.3	132.8
T4	1000	30	30	2.87	1.46	7.0	132.4
T5	1000	40	30	4.45	2.28	4.5	133.5
T6	1000	50	10	4.96	7.33	3.2	132.6
T7	1000	50	20	7.96	5.85	2.4	132.8
EI/C16-MMT							
A1	500	50	30	1.37	0.71	7.9	133.3
A2	1000	50	30	3.17	1.64	5.7	132.5
A3	1700	50	30	8.43	4.27	2.2	132.3
A4	1000	30	30	0.32	0.16	25.2	132.1

[a] Other conditions: 0.5 MPa ethylene, 50 mL hexane, [Zr]=4.0 μmol.
[b] Activity × 10^6 g PE/mol Zr·h.
[c] Calculated by TGA measurement residue at 600°C.
[d] [Zr]=1.0 μmol, 100 mL toluene.

Transmission electron microscopy (TEM) was carried out on a Jeol JEM2200FS transmission electron microscope using an acceleration voltage of 200 KV. Samples for TEM were prepared by embedding in epoxy resin at room temperature and microtomed into ultra-thin sections.

RESULTS AND DISCUSSION

Structures of the EI, CGCT and FI catalysts are displayed in Figure 1.

EI with two cyclopentadienyl anions (Cp) has the tendency to produce lower molecular weight materials under convenient commercial operating conditions. One of the key features of CGCT with one ligand catalyst is the open nature of the catalyst active site which allows them to incorporate other olefins into polyethylene. Meanwhile, compared with the biscyclopentadienyl metallocene (EI), CGCT has increased stability toward MAO, and are remarkably stable up to reaction temperatures of 160°C. Additionally, FI is one of a new family of group IV transition metal complexes possessing a pair of chelating phenoxy-imine ligands, exhibiting high activity for ethylene polymerization. When the three catalysts were supported on OH-C18-MMT,

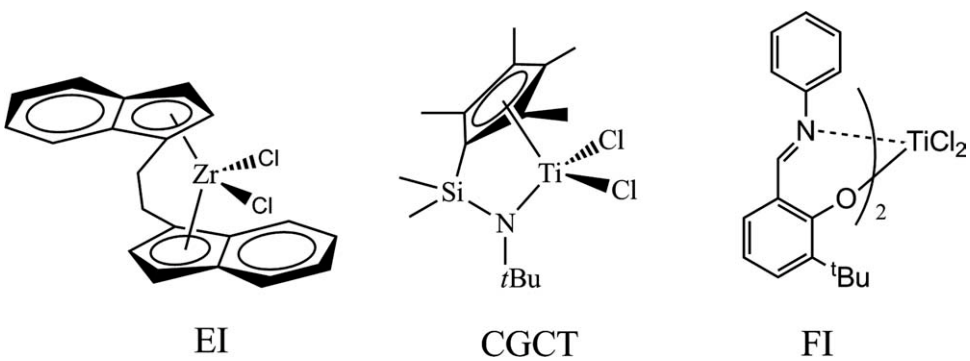

Figure 1 Structures of the catalyst EI, CGCT, and FI.

TABLE II
Characterization Data of the Three OMMTs in Comparison with Na-MMT

Clay	2-Theta (°)	d_{001} (nm)	TGA measurement residue at 600°C (wt %)
Na-MMT	9.06	0.97	≈100
OH-C18-MMT	3.94	2.24	80.8
MMMT	4.12	2.14	80.3
C16-MMT	4.46	1.98	74.4

the ethylene polymerization behavior showed the wide discrepancy among the three supported catalysts due to the different catalyst structures.

Organically modified MMTs (OMMTs) and OMMT-intercalated catalysts

Characterization data of the three OMMTs are shown in Table II, where a comparison is made with those of the pristine Na-MMT. WAXD patterns of the three OMMTs and Na-MMT are plotted in Figure 2(A). All ion-exchange reactions were successful, in spite of the slightly different TGA measurement residues at 600°C [seen in Table II and Fig. 2(B)], indicating that there might be deviations in the ion-exchange reaction using different surfactants. As illustrated in Figure 2(A), distinct shifts of (001) diffraction peak of ordered silicate layers are observed for all OMMTs, OH-C18-MMT at $2\theta = 3.94°$, MMMT at $2\theta = 4.12°$ and C16-MMT at $2\theta = 4.46°$, compared to the pristine Na-MMT at $2\theta = 9.06°$. Accordingly, the d001 values are calculated at 2.24 nm, 2.14 nm, 1.98 nm, and 0.97 nm for OH-C18-MMT, MMMT, C16-MMT, and Na-MMT, respectively. These *d*-spacings (about 2.0 nm) are sufficient for OMMTs to be intercalated effectively by MAO.[26] Because OH groups at the edge of layers of Na-MMT had been reacted by $(CH_3)_3ClSi$ and corresponding CEC value decreased,[27] the d001 interlayer space of organoclay (i.e., MMMT) ionexchanged from chlorosilane-

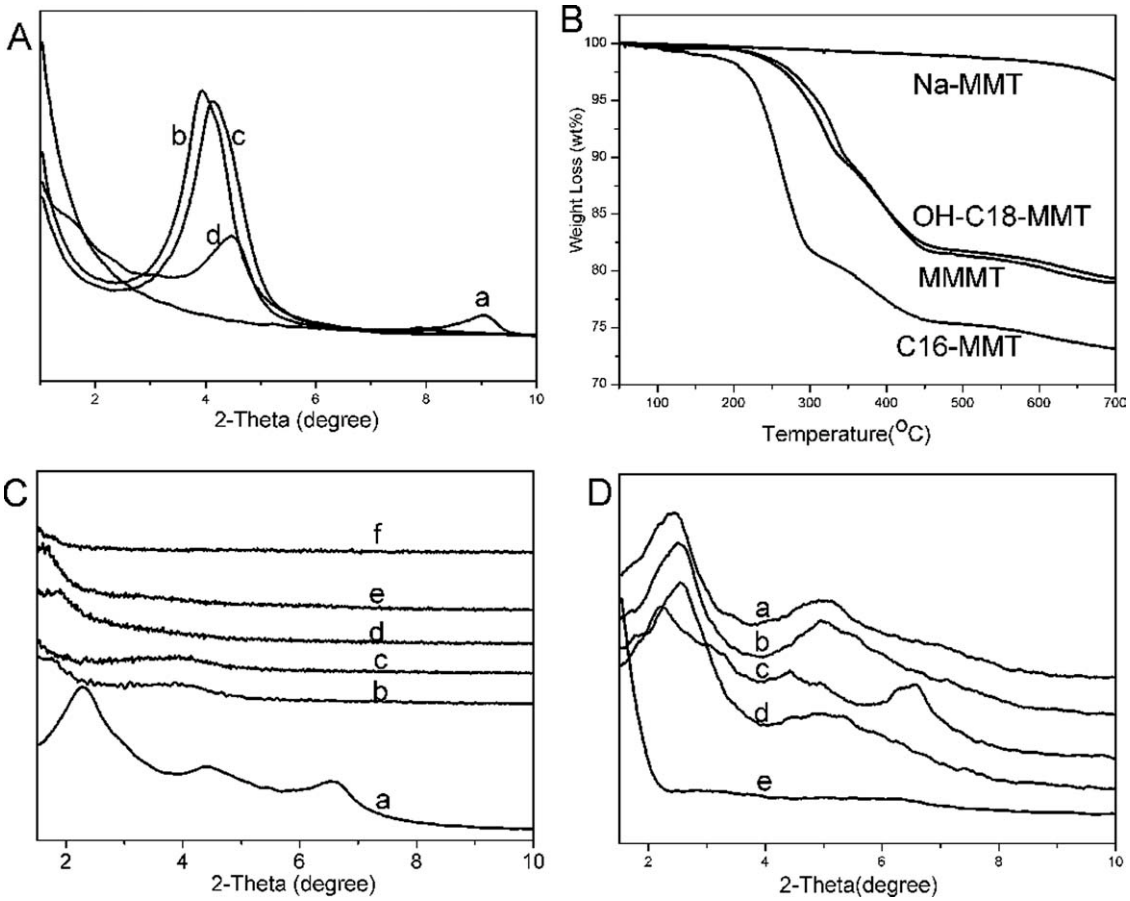

Figure 2 (A) WAXD patterns of: (a) pristine Na-MMT, (b) OH-C18-MMT, cation-exchanged with (2-hydroxylethyl) octadecyldimethyl ammonium nitrate, (c) MMMT, cation-exchanged with trimethylchlorosilane and (2-hydroxylethyl) octadecyldimethyl ammonium nitrate, and (d) C16-MMT, cation-exchanged with hexadecyl trimethylammonium bromide; (B) TGA curves of Na-MMT, OH-C18-MMT, MMMT, and C16-MMT; (C) WAXD patterns of: (a) MAO/C16-MMT 10.0CEC, (b) MAO/OH-C18-MMT 0.5CEC, (c) MAO/OH-C18-MMT 1.0CEC, (d) MAO/OH-C18-MMT 5.0CEC, (e) MAO/OH-C18-MMT 10.0CEC, (f) MAO/OH-C18-MMT 20.0CEC; and (D) WAXD patterns of five OMMT-intercalated catalysts: (a) EI/OH-C18-MMT, (b) EI/MMMT, (c) EI/C16-MMT, (d) CGCT/OH-C18-MMT, and (e) FI/OH-C18-MMT.

TABLE III
A Summary of the OMMT-Intercalated Catalysts

MAO or Cat.	Clay	Feed (g)	Yield of clay support (g)	Cat. /OMMT	Metal content (wt %)[a]
MAO	C16-MMT[b]	6.0	8.4	MAO/C16-MMT	Al/12.7
MAO	OH-C18-MMT[b]	6.0	9.0	MAO/ OH-C18-MMT	Al/17.5
EI	OH-C18-MMT	5.3	7.5	EI/OH-C18-MMT	Zr/0.31
EI	MMMT	5.0	7.2	EI/MMMT	Zr/0.17
EI	C16-MMT	5.5	7.9	EI/C16-MMT	Zr/0.19
CGCT	OH-C18-MMT	5.2	7.4	CGCT/OH-C18-MMT	Ti/0.77
FI	OH-C18-MMT	3.2	5.3	FI/OH-C18-MMT	Ti/0.53

[a] Measured by a titration method.
[b] The amount of MAO is 10.0 CEC.

modified Na-MMT slightly decreased from 2.24 nm to 2.14 nm, seen in Figure 2(A-b,A-c). Comparing OH-C18-MMT [Fig. 2(A-b)] with C16-MMT [Fig. 2(A-d)], it can be clearly seen that the d001 interlayer space of OH-C18-MMT is larger than that of C16-MMT. In all, three different surfactants lead to different d001 interlayer spaces of the final OMMTs, determining the ease of the olefin catalyst intercalation into the interlayers of OMMTs. Figure 2(B) shows the TGA curves of Na-MMT, OH-C18-MMT, MMMT and C16-MMT. Comparing the TGA curve of C16-MMT with that of OH-C18-MMT, the decomposition of C16-MMT began at low temperature and that of OH-C18-MMT started at relatively high temperature, which indicated that the thermal stability of OH-C18-MMT was higher than that of C16-MMT.

The combination of the catalysts (EI, CGCT and FI) with OMMTs (OH-C18-MMT, C16-MMT and MMMT) was completed by the same procedure, i.e., first treating the OMMT with excessive MAO and then allowing the MAO-treated OMMT to react with the metallocene catalyst. To investigate the effect of the hydroxy group during the treatment of OMMTs by MAO, all the intermediates were washed with toluene five times to remove excess MAO after the reaction finished, followed by drying at 60°C in vacuum. The MAO/OH-C18-MMT and MAO/C16-MMT intermediates were subjected to Al content measurement, and the values were seen in Table III. From Table III, the weight of the intermediate product increased compared to original OMMTs. Under the similar reaction conditions (the same reaction temperature, the same reaction time and the 10.0CEC), the increased MAO/C16-MMT weight (2.4 g) was lower than the corresponding MAO/OH-C18-MMT weight (3.0 g), and the Al content in MAO/OH-C18-MMT (17.5 wt %) was higher than that in MAO/C16-MMT (12.7 wt %) (OMMT contains 1.80 wt % of measureable Al). This was because MAO was prior to intercalate into the interlayer of OH-C18-MMT and then the catalysts intercalated.[24] MAO, as cocatalyst, is generally considered to be a mixture of linear and/or cyclic oligomers of different length. Indeed, although alkyl alumoxanes are extensively studied, the MAO cluster structure remains unclear. However, MAO is a very strong Lewis acid and has a site which can react with OH groups in the silicate layers. Thus, it is conceivable that the interaction of MAO chains within the clay galleries originates disordered structures and the weight of OMMTs after MAO treatment increased compared to the OMMT. Figure 2(C) showed that the WAXD patterns of MAO/C16-MMT and MAO/OH-C18- MMT with different amounts of MAO. As shown in Figure 2(C-b–C-f), the intermediates (MAO/OH-C18-OMMT) showed different interlayer distance with different amounts of MAO, which indicated that the OH groups successfully reacted with MAO and intercalated the MAO into interlayer of OH-C18-OMMT. Compared to the XRD pattern of MAO/C16-MMT [Fig. 2(C-a)], MAO/OH-C18-OMMT [Fig. 2(C-e)] had higher interlayer distance of MMT, and it didn't show second or tetra diffraction peak, which gave the evidence that the OH groups played an important role on immobilizing the MAO into interlayer of MMT.

The late transition metals (Zr or Ti) as the active sites of the supporting catalysts were measured via titration method. The OMMTs-based EI catalysts (including EI/OH-C18-MMT, EI/MMMT and EI/C16-MMT) were subjected to Zr content measurement. And both CGCT/OH-C18-MMT and FI/OH-C18-MMT catalysts were subjected to Ti content measurement. These results were given in Table III. From Table III, when the OMMT-intercalated catalysts were compared with the corresponding OMMT, all of the weight increased. In all cases, OMMT was pretreated with different quantities of MAO based on the amount of OMMT used. Although three different surfactants were in the three types of OMMTs, the weight of the final catalysts increased by about 40 wt % compared to the corresponding OMMT. The EI/OH-C18-MMT and CGCT/OH-C18-MMT catalysts increased by about

40 wt %, while the FI/OH-C18-MMT enhanced by 65.6 wt %. Due to the presence of hydroxyl group in the layer of MMT supporter, the Zr content in the final supporting catalyst (EI/OH-C18-MMT) was higher than that without hydroxyl group (EI/C16-MMT). But because the steric hindrance of the edge of layers of MMMT (or the O-Si-C_3H_9 bond existed in the edge of the layers) prevented the active sites of the catalysts (which were embedded in MAO/toluene solutions) from intercalating into the interlayer spaces of MMMT, the Zr content in the EI/MMMT catalyst was lower than that in the EI/OH-C18-MMT catalyst. Under the similar reaction conditions, the different structures of catalysts caused the wide discrepancy of the metal content in the OMMT-intercalated catalysts, and the metal contents were obtained by metal estimation with titration analysis.

Figure 2(D) showed the WAXD patterns of all the OMMTs-intercalated catalysts. As seen from Figure 2(D), the d001 diffraction peaks of OMMTs shifted to a lower angle after the MAO and metallocene catalysts (EI and CGCT) were supported on the corresponding OMMTs, indicating that the metallocene catalysts were successfully intercalated into the interlayer of silicate. For example, the *d*-spacing increased from 2.14 nm in MMMT [Fig. 2(A-c)] to 3.50 nm in EI/MMMT [Fig. 2(D-b)]. In our previous study, we also found that OMMT could absorb MAO and metallocene for intercalation.[24] Seen from the WAXD patterns of the FI/OH-C18-MMT catalyst in Figure 2(D-e), there is a (001) diffraction peak at 3.24° corresponding to the interlayer distance of 2.72 nm, ca.0.48 nm larger than that of the OH-C18-MMT (2.24 nm). By contrast, it is found that EI and CGCT metallocene catalysts with MAO are easy to intercalate into interlayer of OMMT, while such interaction is difficult to occur in the FI catalyst with MAO due to a large steric hindrance.

PE/OMMTs nanocomposites by the OMMTs-intercalated catalysts

The results of ethylene polymerization with the three OMMT-based EI catalysts, EI/OH-C18-MMT, EI/MMMT and EI/C16-MMT, are summarized in Table I. As expected, for all the OMMT-intercalated catalysts, the ethylene polymerization activity (per molar Zr/per hour) depends on the nature of inorganic supports and the catalytic systems, and experimental conditions (including the polymerization solvent, temperature, pressure, time and the concentration of the catalysts, etc). As seen from Table I, the higher [MAO]/[Zr] ratio and the higher temperature could result in higher activity of the OMMTs-intercalated EI catalyst. Among the three OMMT-intercalated catalysts, the catalyst activity at the same [MAO]/[Zr] ratio were different and the order of activity was following EI/C16-MMT<EI/OH-C18-MMT<EI/MMMT. For example, comparing sample T2 with S2 and A2, the activity of EI/MMMT reached to 4.14×10^6 g PE/mol Zr h, while that of the EI/OH-C18-MMT was 3.34×10^6 g PE/mol Zr h and that of the EI/C16-MMT was 1.67×10^6 g PE/mol Zr h. Likewise, under the same polymerization temperature and time, EI/MMMT possessed highest activity among the three different OMMTs-intercalated EI catalysts. For instance, EI/MMMT displayed much higher activity (1.46×10^6 g PE/mol Zr h) than the other two catalysts EI/OH-C18-MMT (0.64×10^6 g PE/mol Zr h) and EI/C16-MMT (0.16×10^6 g PE/mol Zr h) under the polymerization temperature of 30°C. This could be attributed that the use of a mixed TM and OH-C18 surfactant in the cation-exchanged organic modification of MMT not only provided catalyst-anchoring reactive sites to facilitate the stabilization of catalyst species in MMT interlayer gallery but also helped to create a catalytically benign environment for the intercalated metallocenes to fully exert its catalytic function on polymerization. Comparing entry T6, T7 with T2, for EI/MMMT, catalyst activity decreased with the increase of reaction time as expected. This adds complexity in controlling nanocomposite composition by simple polymerization time adjustment.

Ethylene polymerization was performed with the OH-C18-MMT-intercalated CGCT and FI catalysts as well as the corresponding homogenous catalysts, and the results were shown in Table IV. It is well known that metallocene catalysts such as EI and CGCT could catalyze ethylene to produce polyethylene with a high polymerization activity. In addition, FI possesses a pair of chelating phenoxy-imine ligands and displays high catalytic performance for the polymerization of ethylene. Under the similar reaction conditions, the activity of FI for ethylene homopolymerization (8.08×10^6 g PE/mol Ti h) is much higher than that of CGCT (1.97×10^6 g PE/mol Ti h).

As expected, all three catalysts supported on OH-C18-MMT displayed lower activities for ethylene polymerization than the corresponding homogenous catalysts, as seen in Table IV. The activity of ethylene polymerization by the CGCT/OH-C18-MMT catalyst (0.71×10^6 g PE/mol Ti h) was much lower than that by the CGCT catalyst (1.97×10^6 g PE/mol Ti h). However, when FI was supported on OH-C18-MMT, the activity of ethylene polymerization was obviously much lower than the corresponding homogeneous activity. For example, the catalytic activity of FI/OH-C18-MMT for ethylene polymerization only reached to 0.04×10^6 g PE/mol Ti h under the polymerization temperature of 50°C. This may be attributed that asymmetric ligands of FI catalysts possess a large steric hindrance for the Ti metal

TABLE IV
Summary of Ethylene Polymerization Using the Two Different Catalysts

Entry.	[Ti] (umol)	T (°C)	t (min)	Yield (g)	A[a]	MMT[b] (wt%)	T_m (°C)
homogeneous CGCT							
PE2	5.0	50	20	3.28	1.97	–	133.8
CGCT/OH-C18-MMT							
C1	5.0	50	30	2.35	0.94	9.0	133.7
C2	5.0	50	60	3.56	0.71	5.3	133.9
C3	5.0	30	60	1.14	0.23	17.5	133.6
homogeneous FI							
PE3[c]	1.0	50	30	4.04	8.08	–	134.2
FI/OH-C18-MMT							
F1	29.0	50	30	0.597	0.04	33.1	131.1
F2	28.0	70	30	0.697	0.05	23.5	132.4

Reaction conditions: 50 mL hexane, 0.5 MPa.
[a] Activty$\times 10^6$g PE/mol Ti·h.
[b] Calculated by TGA measurement residue at 600°C.
[c] 100 mL toluene.

center after the FI catalyst was immobilized in OH-C18-MMT, which lessens the opportunities for the ethylene monomers approaching into the active sites in the interlayer galleries of OH-C18-MMT.

Characterization of PE/OMMTs nanocomposites

The thermal properties of PE/OMMT nanocomposites are investigated by TGA and DSC, and the results are summarized in Table I, Table IV and Figure 3. Figure 3(A) shows the DSC curves of PE/OMMTs nanocomposites. For all PE/OMMT nanocomposites, the melting temperatures (T_m) are equal or slightly differential in agreement with our previous research.[24] But T_m values of the PE/OMMT nanocomposites prepared by OMMTs-intercalated EI catalysts (seen in Table I) are slightly higher than that of PE1 prepared without MMT (131.4°C). However, a decrease of T_m is observed for the composites by FI/OH-C18-MMT containing high MMT content (sample F1 and sample F2 in Table IV) compared to that of PE3 without MMT. As seen from Figure 3(A), the melting temperatures of PE/OH-C18-MMT nanocomposites slightly decreased with the increase of MMT contents in PE matrix, but T_ms of PE/C16-MMT slightly increased with the increase of MMT contents. The WAXD patterns of the nanocomposites [Fig. 4(A)] also reveal that the PE matrix crystallized, as they show diffraction peaks at $2\theta = 21.5$ and 23.9 corresponding to the crystallite planes of 200 and 110.

Figure 3(B) presents the TGA curves of PE/OMMTs with different types of OMMT and catalysts. Seen from Figure 3(B-f), the TGA trace of

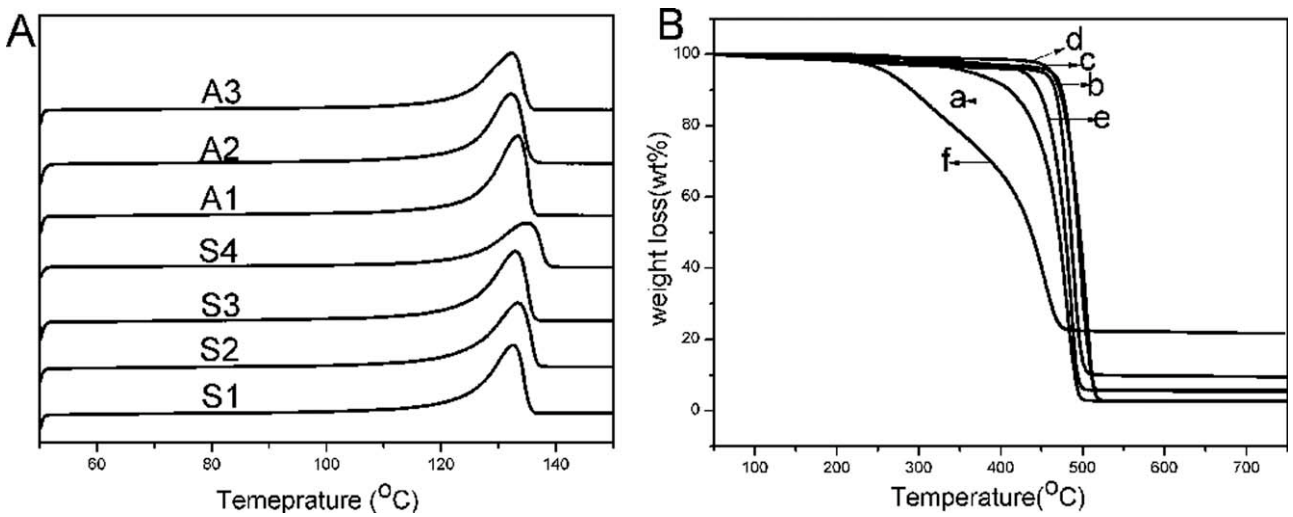

Figure 3 (A) DSC curves of PE/OMMT nanocomposites; and (B) TGA curves of PE/OMMT nanocomposites, (a) sample S2 with 2.8 wt % MMT, (b) sample S5 with 9.8 wt % MMT, (c) sample T2 with 2.9 wt % MMT, (d) sample A5 with 5.7 wt % MMT, (e) sample C2 with 5.3 wt % MMT, and (f) sample F2 with 23.5 wt % MMT.

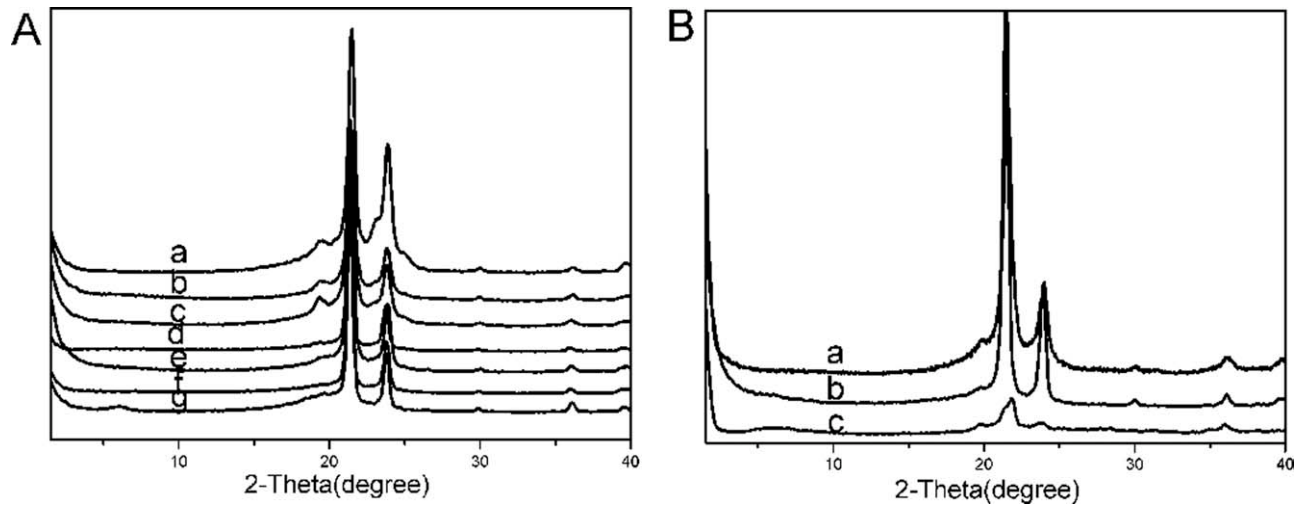

Figure 4 XRD patterns of the PE/OMMT nanocomposites (A): (a) sample S2, (b) sample S5, (c) sample T2, (d) sample T4, (e) sample A1, (f) sample A2, and (g) sample A4; (B): (a) sample C1, (b) sample C2, and (c) sample F2.

sample F2 with 23.5 wt % MMT by FI/OH-C18-MMT is characterized by two-stage decomposition. Low-temperature weight loss is partially ascribed to the degradation of the organic modifier due to highly filled amount of OMMT in PE-based hybrid without exfoliation or disorder. The major peak is due to the degradation of polyethylene chains. However, only one decomposition peak appeared in TGA curves of other nanocomposites. The degradation behavior of composites is obviously sensitive to the synthesis parameters. It is noted that the PE-based hybrid with 9.8 wt % MMT [seen in Fig. 3(B-b)] are more thermally stable than those with 2.8 wt % MMT [seen in Fig. 3(B-a)], which could be attributed that a physical barrier effect of the nanodispersed silicate layers in PE matrix enhanced with the increase of MMT content. From the melting temperatures and TGA curves of the final polymer nanocomposites, we could conclude that ethylene polymerization occurring in a confined environment would more or less influence the polymer chain propagation and the structure of the resulting polymer.

WAXD patterns of all PE/OMMTs nanocomposites were recorded in 2θ ranges of 1.5–40°, as seen in Figure 4. From Figure 4(A-b), it was found that, although the MMT content in PE matrix is high to 9.8 wt %, the XRD curves of PE/OMMTs nanocomposites (sample S5) catalyzed by EI/OH-C18-MMT displayed no (001) diffraction peak from MMT, indicating that the average interlayer space of the MMT in the PE matrices was larger than 5.8 nm according to the Bragg equation. Similar WAXD patterns were obtained for other PE/OH-C18-MMT nanocomposites [sample S2 seen in Fig. 4(A-a), sample S1, S3, S4 and S6 not shown] by EI/OH-C18-MMT. And there are no *d*001 diffraction peaks in the WAXD patterns of sample T2 and T4 by EI/MMMT [seen in Fig. 4(A-c,A-d)]. This reflects the advantages of the *in situ* polymerization for the preparation of polyolefin/clay nanocomposites, i.e., contributing to good exfoliation and homogenous dispersion of silicate layers in the PP matrix during the process of PP chains growth accompanied with the release of polymerization heat. And the XRD curves of the sample A1 and A2 by EI/C16-MMT also presented no (001) diffraction peak from MMT [see Fig. 4(A-e,A-f)]. However, for the PE/C16-MMT nanocomposite (sample A4) with 25.2 wt % MMT, its WAXD pattern displays a strong (001) diffraction peak at the angular region of $2\theta = 6.0°$ [see Fig. 4(A-g)], indicating that at least the majority of the silicate layers of OMMT is agglomerate because of the large amount of OMMT in PE matrix.

Seen from Figure 4(B-c), for the PE/OH-C18-MMT nanocomposites (sample F2) prepared by FI/OH-C18-MMT, because FI/OH-C18-MMT displayed low activity for ethylene polymerization so that a large amount of OH-C18-MMT were existed in the final PE matrix, there is a strong and broad (001) diffraction peak at $2\theta = 5.0–7.5°$ in its WAXD pattern. On the contrary, the PE/OH-C18-MMT nanocomposites with 9.0 wt % and 5.3 wt % MMT by CGCT/OH-C18-MMT displayed no d001 diffraction peak in their WAXD patterns [see Fig. 4(B-a,B-b)].

The TEM images of PE/OMMT nanocomposites are shown in Figure 5. As can be seen from Figure 5, even though the content of nanosilicate is higher than 5.0 wt %, the silicate layers are dispersed uniformly in the whole PE matrix, and micron-sized clays are scarcely observed in the PE matrix. The TEM image of sample S3 [Fig. 5(A)] with 1.5 wt % MMT showed a few exfoliated silicate layers. It can be concluded from both TEM and XRD

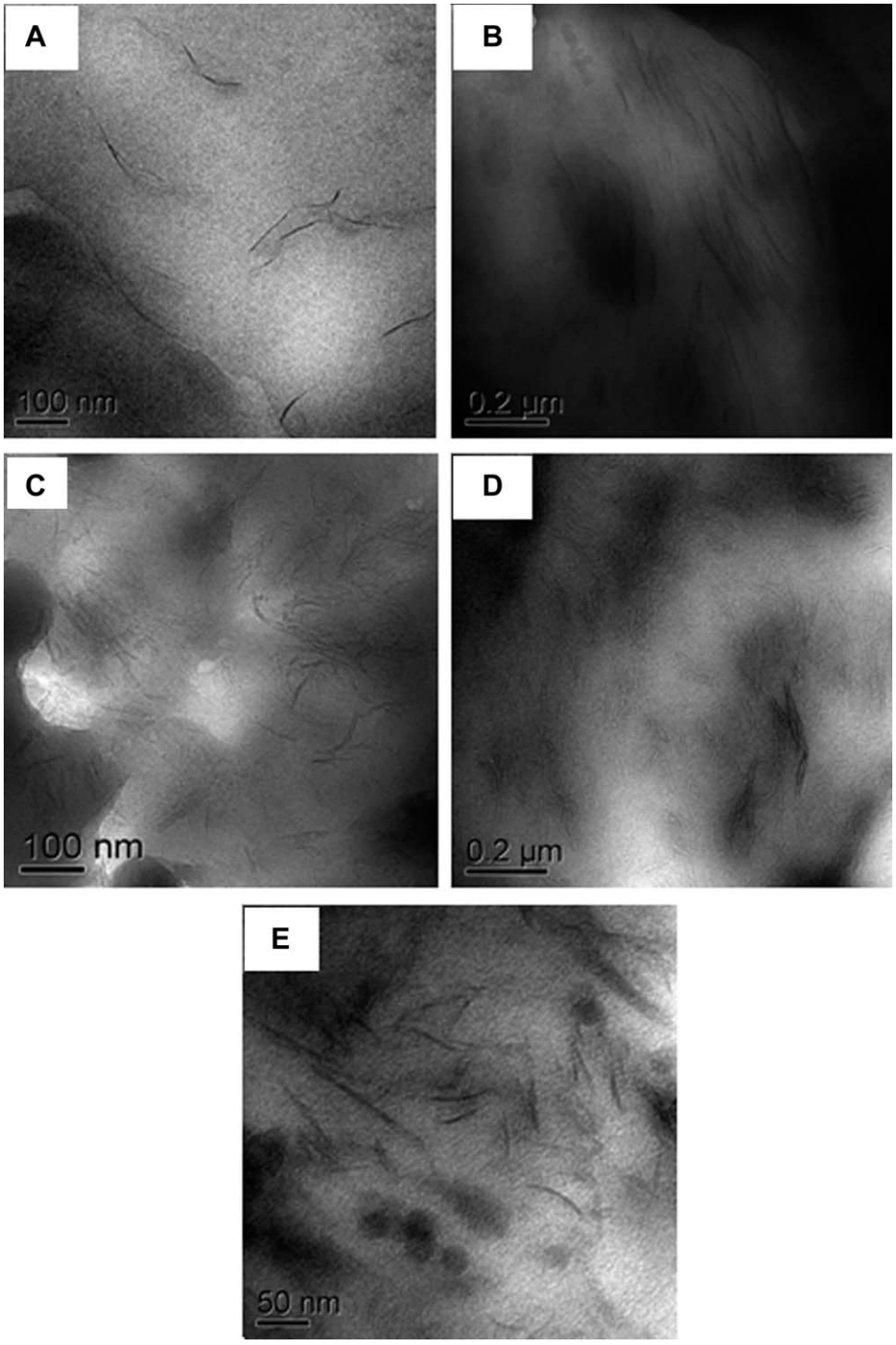

Figure 5 TEM image of PE/OMMT nanocomposites, (A) sample S3, (B) sample S5, (C) sample T4, (D) sample A1, and (E) sample C2.

measurements that the silicate layers are well exfoliated and homogeneously dispersed in the PE matrix.

CONCLUSIONS

In summary, the EI catalyst was supported on the different OMMTs modified by three different surfactants, (2-hydroxylethyl) octadecyl dimethylammonium nitrate as single-functionalized surfactant (remarked as OH-C18-MMT), trimethylchlorosilane and (2-hydroxylethyl) octadecyl dimethylammonium nitrate as a mixed surfactant (remarked as MMMT), and hexadecyl trimethylammonium bromide as nonfunctionalized surfactant (remarked as C16-MMT), to prepare PE hybrids by *in situ* intercalative

polymerization. EI/MMMT showed higher activity than EI/OH-C18-MMT and EI/C16-MMT under the similar polymerization conditions, indicating that the use of the mixed surfactant in the cation-exchanged organic modification of MMT helped to create a catalytically benign environment for the intercalated EI catalyst to fully and efficiently exert its catalytic function on ethylene polymerization. Although FI, as a new family of IV transition metal complexes owning a pair of chelating phenoxy-imine ligands, had a high activity for ethylene homopolymerization, it displayed low activity after it being supported on OH-C18-MMT due to the presence of OH-C18-MMT. Its activity was so obviously low that the content of OH-C18-MMT in PE matrix was high and the silicate layers agglomerated in it. Compared with the FI catalyst, the EI and CGCT catalysts showed higher activities in the presence of OH-C18-MMT. PE/OMMT nanocomposites with good exfoliation and homogeneous dispersion of MMT were obtained and the results were seen in WAXD and TEM characterizations.

References

1. Kawasumi, M. J Polym Sci Part A: Polym Chem 2004, 42, 819.
2. Usuki, A.; Hasegawa, N.; Kato, M. Adv Polym Sci 2005, 179, 135.
3. Galli, P.; Vecellio, G. J Polym Sci Part A: Polym Chem 2004, 42, 396.
4. Lee, D. H.; Kim, H. S.; Yoon, K. B.; Min, K. E.; Seo, K. H.; Noh, S. K. Sci Technol Adv Mater 2005, 6, 457.
5. Manias, E.; Touny, A.; Wu, L.; Strawhecker, K.; Lu, B.; Chung, T. C. Chem Mater 2001, 13, 3516.
6. Dubois, P.; Alexandre, M.; Jérôme, R. Macromol Symp 2003, 194, 13.
7. Liu, C. B.; Tang, T.; Wang, D.; Huang, B. T. J Polym Sci Part A: Polym Chem 2003, 41, 2187.
8. Rong, J. F.; Li, H. Q.; Jing, Z. H.; Hong, X. Y.; Sheng, M. J Appl Polym Sci 2001, 82, 1829.
9. Jin, Y. H.; Park, H. J.; Im, S. S.; Kwak, S. Y.; Kwak, S. J. Macromol Rapid Commun 2002, 23, 135.
10. Jungling, S.; Koltzenburg, S.; Mulhaupt, R. J Appl Polym Sci 1997, 35, 1.
11. Chu, K. J.; Soares, J. B. P.; Penlidis, A. J Polym Sci A: Polym Chem 2000, 38, 462.
12. Wang, Q.; Zhou, Z.; Song, L.; Xu, H.; Wang, L. J Polym Sci Part A: Polym Chem 2004, 42, 38.
13. Liu, C.; Tang, T.; Huang, B. J Catal 2004, 221, 162.
14. Alexander, M.; Dubois, P.; Sun, T.; Garces, J. M.; Jerome, R. Polymer 2002, 43, 2123.
15. Heinemann, J.; Reichert, P.; Thomann, R.; M̈lhaupt, R. Macromol Rapid Commun 1999, 20, 423.
16. Ray, S.; Galgali, G.; Lele, A.; Sivaram, S. J Polym Sci Part A: Polym Chem 2005, 43, 304.
17. Bergman, J. S.; Chen, H.; Giannelis, E. P.; Thomasc, M. G.; Coates, G. W. Chem Commun 1999, 21, 2179.
18. Leone, G.; Bertini, F.; Canetti, M.; Boggioni, L.; Stagnaro, P.; Tritto, I. J Polym Sci Part A: Polym Chem 2008, 46, 5390.
19. Leone, G.; Bertini, F.; Canetti, M.; Boggioni, L.; Conzatti, L.; Tritto, I. J Polym Sci Part A: Polym Chem 2009, 47, 548.
20. Yang, K. F.; Huang, Y. J.; Dong, J. Y. Chin Sci Bull 2007, 52, 181.
21. He, A.; Hu, H.; Huang, Y.; Dong, J. Y.; Han, C. C. Macromol Rapid Commun 2008 2004, 25.
22. Huang, Y.; Yang, K.; Dong, J. Y. Macromol Rapid Commun 2006, 27, 1278.
23. Huang, Y.; Yang, K.; Dong, J. Y. Polymer 2007, 48, 4005.
24. Yang, K. F.; Huang, Y. J.; Dong, J. Y. Polymer 2007, 48, 6254.
25. Saito, J.; Mitani, M.; Matsui, S.; Tohi, Y.; Makio, H.; Nakano, T.; Tanaka, H.; Kashiwa, N.; Fujita, T. Macromol Chem Phys 2002, 203, 59.
26. Sano, T.; Doi, K.; Hagimoto, H.; Wang, Z.; Uozumi, T.; Soga, K. Chem Commun 1999, 733.
27. Zhao, C.; Feng, M.; Gong, F.; Qin, H.; Yang, M. J Appl Polym Sci 2004, 93, 676.